Silicon-Based Integrated Inductors for Wireless Applications

Bruce C. Kim*
*Department of Electrical Engineering
*Arizona State University
E-mail : bruce.kim@asu.edu

ABSTRACT

This paper presents circuit modeling and characterization of silicon-based on-chip integrated inductors in Giga Hertz range for wireless communication products. We compare several different designs of on-chip inductors for self-resonant frequency and quality factor. The measurement data could be used as a design guide for manufacturing practical spiral inductors for wireless applications. We provide the equivalent inductor circuit parameters from the actual measurement data.

Key words
Silicon, Intergrated Inductors, Wireless,

I. INTRODUCTION

In recent wireless communications market, there is a high demand for reduced size, high performance, low power and low cost wireless products. In order to meet these market demands, many off-chip passive devices are being moved to on-chip as integrated passives. Inductors are very important passive elements in many circuit applications such as resonator tank circuits, narrow-band impedance matching, low noise degeneration and feedback, linear filters and baluns [1, 2].

High quality inductors are required to achieve low power, low noise, and wide bandwidth wireless applications [3]. There are numerous papers on design and fabrication of integrated inductors for wireless applications [4-7]. However, the inductors fabricated on a lossy silicon-based substrate provide low quality factor (Q), typically less than 5. We have shown that the Q of on-chip inductors can be made up to 35 on a very high-resistivity silicon substrates [8]. We measured several different types of inductors and compared the results. We show simple circuit parameter extraction procedures to characterize the inductors.

II. MEASUREMENTS

(A) Quality factor and self-resonant frequency

We measured several on-chip spiral inductors on a very high resistivity substrate with HP-8510 network analyzer and Cascade probe station. The measurement system was calibrated with LRRM technique. The scattering parameters were then converted to admittance parameters as shown in Eq. (1) [9].

$$[y]=[Y_0]([1]-[s])([1]+[s])^{-1} \quad (1)$$

$$\text{where} \quad [Y_0]=\begin{bmatrix} Y_0 & 0 \\ 0 & Y_0 \end{bmatrix} \quad (2)$$

The parasitics of the inductor pads were de-embedded using the open structure on the same substrate. The admittance parameters of the inductor itself were obtained by subtracting out the open structure admittance parameters from the spiral inductor admittance parameters. The quality factor of the measured inductors was calculated by traditional method [10].

$$Q=-\frac{Im(y_{11})}{Re(y_{11})} \quad (2)$$

The quality factor was plotted as the function of frequency as shown in Fig. 1. The self-resonant frequency was determined by the quality factor at the point where Q becomes zero. For example, the maximum quality factor of the

30nH octagonal inductor shown in Fig. 1 is approximately 19, and the self-resonant frequency is at 1.9GHz. Normally, the inductor would operate at the maximum Q point which is far away from the self resonant frequency.

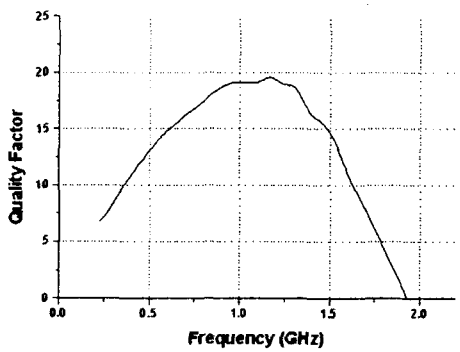

Fig. 1 Quality factor vs. frequency of a 30nH octagonal inductor.

(B) Extraction of the equivalent circuit parameters

The equivalent circuit of two-port spiral inductor is shown in Fig. 2 [10]. The series branch consists of the serial inductance L_S, the serial resistance RS, and the series feed forward capacitor C_S. Two parallel branches represent parasitics of port-1 and port-2. The capacitor C_{OX} represents the capacitance between the spiral turns of inductor and the substrate. The silicon substrate is modeled by CSUB and RSUB.

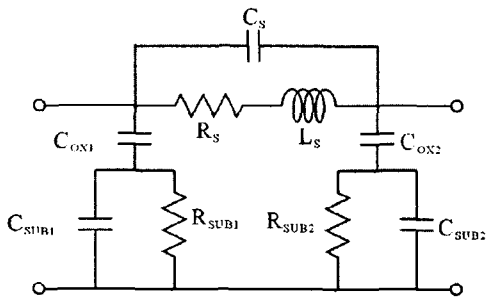

Fig. 2. Equivalent circuit of two-port inductor.

We used optimization technique to find the equivalent circuit parameters. It is not easy to optimize the nine unknown circuit parameters from the beginning. Therefore, we simplified the two-port equivalent circuit as -model as shown in Fig. 3. The Y_1, Y_2 and Y_3 in the -model were calculated from the admittance values from the [y] matrix in Equation (1).

$$Y_1 = y_{11} + y_{12} \tag{3.a}$$

$$Y_2 = y_{21} + y_{12} \tag{3.b}$$

$$Y_3 = -y_{12} \tag{3.c}$$

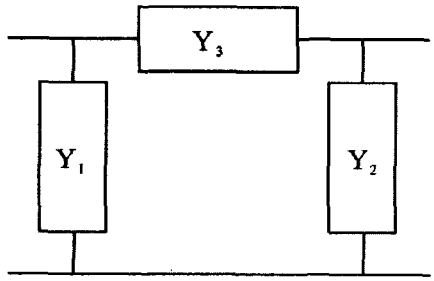

Fig. 3. Pi-model for two-port integrated inductor.

The series branch Y_3 includes R_S, L_S, and C_S. The shunt branches Y_1 and Y_2 include the C_{OX}, C_{SUB} and R_{SUB}. This allowed us to simplify the optimization from nine to three elements. We used commercial software (Agilent ADS) for running the optimization problem. The initial values are important in optimization technique. We used the simplified equivalent circuit to calculate the initial values as shown in Fig. 4. The values of C_S, C_{SUB1}, and C_{SUB2} were omitted in this circuit because these values were very small. The initial values of the equivalent circuit parameters can be found by using the equations shown in Equation (4.a 4.f).

$$R_s = \mathrm{Re}\left(-\frac{1}{y_{12}}\right) \tag{4.a}$$

$$L_s = \frac{1}{\omega}\,\mathrm{Im}\left(-\frac{1}{y_{12}}\right) \tag{4.b}$$

$$R_{SUB1} = \mathrm{Re}\left(\frac{1}{y_{11}+y_{12}}\right) \tag{4.c}$$

$$C_{OX1} = -\frac{1}{\omega}\,\frac{1}{\mathrm{Im}\left(\frac{1}{y_{11}+y_{12}}\right)} \tag{4.d}$$

$$R_{SUB2} = \mathrm{Re}\left(\frac{1}{y_{22}+y_{21}}\right) \tag{4.e}$$

$$C_{OX2} = -\frac{1}{\omega}\,\frac{1}{\mathrm{Im}\left(\frac{1}{y_{22}+y_{21}}\right)} \tag{4.f}$$

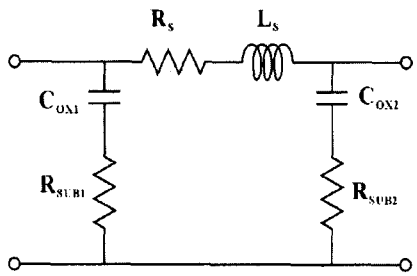

Fig 4. Simplified equivalent circuit of the inductor.

The following procedure shows simple steps to extract the equivalent circuit parameters.

1. Measure the scattering parameters of the inductor.
2. Measure the scattering parameters of open structure.
3. Convert measured scattering parameters to admittance parameters.
4. De-embed the pad parasitics.
5. Find Y_1, Y_2, and Y_3.
6. Calculate the scattering parameters for Y_1, Y_2, and Y_3, respectively.
7. Optimize the Y_1, Y_2, and Y_3 using ADS.

Table 1 shows the optimized values of the circuit parameters for the inductor model shown in Fig. 2.

Table 1. Extracted parameter values for inductor.

Circuit parameter	Extracted value
L_S	6.66 nH
R_S	2.82 W
C_P	0.216 pF
C_{OX1}	0.597 pF
R_{SUB1}	61.2 kW
C_{SUB1}	0.130 pF
C_{OX2}	0.592 pF
R_{SUB2}	99.9 kW
C_{SUB2}	0.106 pF

III. RESULTS

We fabricated numerous shapes of spiral inductors on the wafer. In this paper, we concentrate on the inductors with and without ground shields. We characterized inductors for maximum Q values and self-resonant frequencies. Figure 5 illustrates details of physical parameters for spiral inductors that we studied. They are length, width, diameter and space. Figures 6(a), 6(b), 6(c) and 6(d) show the fabricated spiral inductors. We used these types of inductors for the measurements.

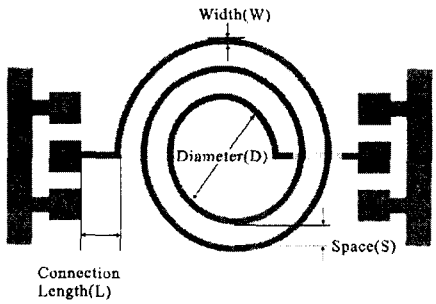

Fig. 5 The sketch of circular spiral inductor with 2.5 turns.

Figure 7 shows measured Q values for several different spiral inductors. In this measurement, we used inductors with 2 to 5 turns. From the figure, we can summarize that one-port inductors with ground shields have a higher quality factor than those without ground shields. Furthermore, one-port inductors have higher quality factor than two-port inductors. As expected, the inductors with longer line between the pad and the inductor have a smaller quality factor than those with shorter connection line. The quality factors with varying inner diameter of the spiral inductor are shown in Fig. 8. The inner diameter of the spiral inductors has little influence on the maximum quality factor.

The measured self-resonant frequency with varying number of turns is shown in Fig. 9. Two-port inductors have lower self- resonant frequency than one-port inductors as shown in the bars (a) and (c) of Fig. 9.

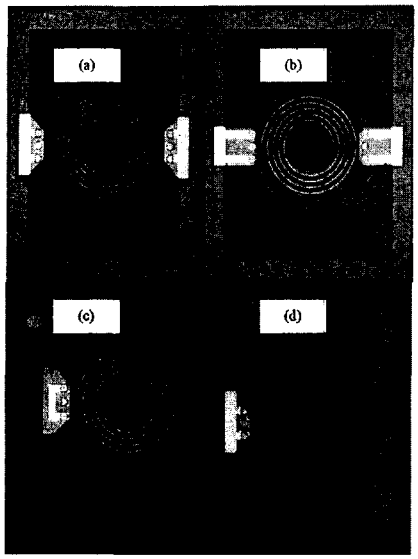

Fig. 6 (a) shielded two-port spiral inductor with normal length between pad and the inductor, (b) shielded two-port spiral inductor with short length between pad and inductor, (c) single port spiral inductor without ground shield, (d) single port spiral inductor with ground shield.

The self-resonant frequency decreases as the number of spiral turns increases. This is due to increase in parasitic capacitance (CS) as the number of spiral turns increases. Therefore, the self-resonant frequency is decreased as the number of turns increases. The self-resonant frequency has little relationship with the space as shown in the data of Fig. 9. From Fig. 10, we can see that the self-resonant frequency decreases as the inner diameter of spiral increases.

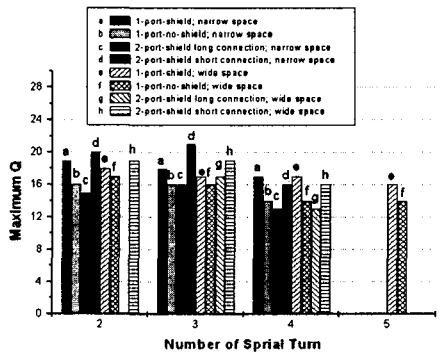

Fig. 7. Q measurements on different types of spiral inductors.

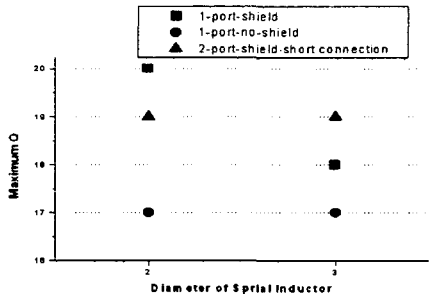

Fig. 8. Q measurements with varying diameters.

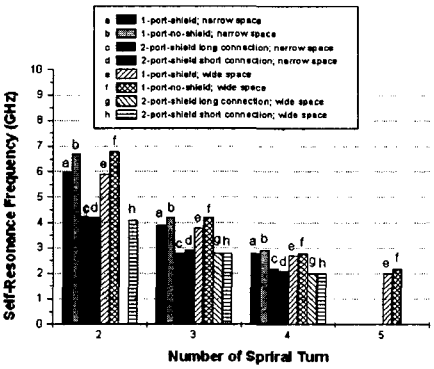

Fig. 9. Measurements of self resonant frequencies on varying spiral turns.

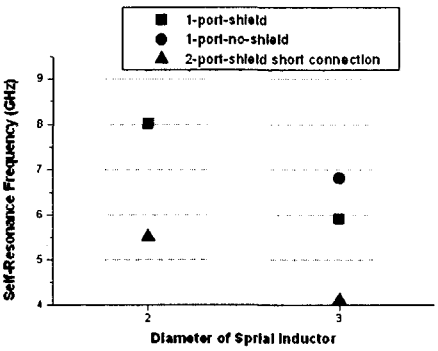

Fig. 10. Measurements of self-resonant frequency with varying diameters.Fig.

IV. CONCLUSIONS

his paper presents modeling and characterization of silicon-based on-chip inductors for wireless communication products. We

measured several spiral inductors with varying parameters. The measurement shows that one -port inductors with ground shields have higher quality factor than those without ground shields. The self-resonant frequency decreases as the number of turns increases. We introduced optimization procedure for obtaining equivalent circuit parameters of spiral inductors from measured S-parameters.

REFERENCES

[1] J.A. Power, S.C. Kely, E.C.Griffith, and M. O'Neil, An investigation of on-chip spiral inductors on a 0.6 m BiCMOS technology for RF applications, Proc. IEEE on Microelectronic Test Structure, vol. 13, pp. 18-23, March 1999

[2] Yeong J. Yoon, Yicheng Lu, Robert C Frye, and Peter R. Smith, Modeling of monolithic RF Spiral transmission line balun, IEEE Trans. Microwave Theory Tech., vol. 49, pp. 393-395

[3] P. Pieters, K. Vaesen, S. Brebels, S. Mahmoud, W. Raedt, E. Beyne, and R. Mertens, Accurate Modeling of High-Q Spiral Inductors in Thin-Film Multilayer Technology for Wireless Telecommunication Applications, IEEE Trans. Microwave Theory Tech. vol. 49, pp. 589-599, April 2001

[4] H.M. Hsu, et. al., Silicon integrated high performance inductors in a 0.18 m CMOS technology for MMIC, Symposium on VLSI Circuits, 2001.

[5] Y.K. Koutsoyannopoulos, Y. Papananos, Systematic analysis and modeling of integrated inductors and transformers in RF IC design, IEEE Transactions on Circuits and Systems II: Analog and Digital Signal Processing, vol. 47 , Aug. 2000

[6] Lopez-Villegas, J.M.; Samitier, J.; Cane, C.; Losantos, P.; Bausells, J., Improvement of the quality factor of RF integrated inductors by layout optimization, IEEE Trans. Microwave Theory Tech., vol. 48, Jan. 2000.

[7] Arcioni, P.; Castello, R.; De Astis, G.; Sacchi, E.; Svelto, F., Measurement and modeling of Si integrated inductors, IEEE Trans. Instrum. Meas., Vol. 47, Oct. 1998.

[8] B. Kim, D. Han, R. Liu, Y. Yoon, Characterization and Testing on Integral Passives for Wireless Applications, IEEE 8th International Advanced Packaging Materials Symposium, March 2002.

[9] David M. Pozar, Microwave Engineering, John Wiley & Sons, Inc 1988

[10] Ali M. Niknejad, and Robert G. Meyer, Analysis, Design, and Optimization of Spiral Inductors and Transformers for Si RF IC's, IEEE J. of Solid-State Circuits, vol. 33, pp. 1470-1481, Oct. 1998]